Gobikrishnan et al. 2025. *Int. J. Vehicle Structures & Systems*, 17(4), 639-646
ISSN: 0975-3060 (Print), 0975-3540 (Online)
doi: 10.4273/ijvss.17.4.15

International Journal of Vehicle Structures & Systems
Available online at https://yanthrika.com/eja

Optimization of Corrosion Resistance in AA7075 using Hybrid Si-Zr Sol-Gel Coatings Doped with Cerium Nitrate using Taguchi Method

U. Gobikrishnan[a], Pon Maheskumar[b], A. Ravi[c], P.S.V.S. Sridhar[d], M. Vigneshwaran[e] S. Nanthakumar[f], Tarun Kumar Kotteda[g], Chitharthan Shanmugam[h], M. Anil Kumar[g] and R. Girimurugan[b,i]

[a]*Dept. of Mech. Engg., Sona College of Tech., Salem, Tamil Nadu, India*
[b]*Dept. of Mech. Engg., Nandha College of Tech., Perundurai, Tamil Nadu, India*
[c]*Dept. of Electrical and Electronics Engg., K S R College of Engg., Tiruchengode, Tamil Nadu, India*
[d]*Dept. of Computer Sci. and Engg., Koneru Lakshmaiah Education Foundation, Vaddeswaram, Andhra Pradesh, India*
[e]*Dept. of Mechatronics Engg., Sri Krishna College of Engg. and Tech., Coimbatore, Tamil Nadu, India*
[f]*Dept. of Mech. Engg., PSG Inst. of Tech. and Applied Res., Coimbatore, Tamil Nadu, India*
[g]*Dept. of Mech. Engg., Sagi Rama Krishnam Raju Engg. College, Bhimavaram, Andhra Pradesh, India*
[h]*Dept. Of Mech. Engg, Karpagam College of Engg., Coimbatore, Tamil Nadu, India*
[i]*Corresponding Author, Email ID: dr.r.girimurugan@gmail.com*

ABSTRACT:

In this investigation, the Taguchi method was applied to experimental design to ascertain the most favourable parameters for a hybrid sol-gel coating composed of Si-Zr and cerium nitrate. Each of the five independent variables in the experimental design had four possible values. It employed an L16 orthogonal array. The purpose of these trials was to find the ideal sol-gel deposition settings for AA7075. The chemical arrangement of hybrid films was studied with attenuated total reflectance Fourier transform infrared spectroscopy. Using a potential-dynamic polarization testing, the corrosion rate of the coatings was assessed. Analysis of variance was employed to predict the optimal processing parameters based on data analysis and the signal-to-noise ratio. Applying the optimal experimental conditions resulted in a five-fold reduction in the corrosion rate of coated AA7075 relative to uncoated AA7075.

KEYWORDS:

AA7075; Corrosion rate; Taguchi method; Coatings; Signal-to-noise ratio

CITATION:

U. Gobikrishnan, P. Maheskumar, A. Ravi, P.S.V.S. Sridhar, M. Vigneshwaran, S. Nanthakumar, T.K. Kotteda, C. Shanmugam, M.A. Kumar and R. Girimurugan. 2025. Optimization of Corrosion Resistance in AA7075 using Hybrid Si-Zr Sol-Gel Coatings Doped with Cerium Nitrate using Taguchi Method, *Int. J. Vehicle Structures & Systems*, 17(4), 639-646. doi:10.4273/ijvss.17.4.15.

1. Introduction

Aluminium alloy (AA) finds extensive use in aerospace and maritime applications due to its exceptional characteristics. When these alloys are exposed to environments that include chloride, they corrode [1]. Chemical conversion coatings based on chromium (VI) are the most popular choice for improving aluminium's corrosion resistance. Chromate conversion coating has the main drawback of being hazardous to humans due to Cr (VI). These substances are known to cause cancer. Hexavalent chromium interferes with cellular processes and can be absorbed through the lungs and skin [2]. Non-toxic alternatives to traditional protective coatings for AA are presented in the form of organic-inorganic hybridized films made through the sol-gel Technology. These materials have piqued the curiosity of coating scientists in the past 10 years [3]. The sol-gel method involves a great deal of experimental variables, however and these parameters impact the coating qualities, particularly its corrosion resistance. Our previous research [4] demonstrated that the adhesive strength and barrier properties of glycidoxypropyl-trimethoxy-silane (GPTMS), tetra-ethyl-orthosilicate (TEOS) hybrid coatings are influenced by the quantities of zirconium and cerium present. Therefore, it is difficult to prepare an appropriate coating and a great number of trials need to be conducted. It makes sense to use a statistical strategy such as Taguchi method to reduce the number of trials because conducting all of them is costly and time-consuming. Very little research has focused on determining the optimal settings to achieve the best corrosion behaviour. The aim of this study was to optimize the parameters of the sol-gel method in order to fabricate an anti-corrosion coating on a substrate made of AA7075. GPTMS and TEOS with zirconium (IV) n-propoxide and cerium inhibitor would comprise this coating. The optimization was accomplished with the Taguchi design. The impact of several variables on the corrosive rate of coating AA7075 was discussed.

2. Experimental methodology

By applying the DOE experimental methodology, which is founded on the Taguchi method, the influence of

processing factors on the rate of coating deterioration was examined. Out of four levels, five parameters were chosen for the methodology of the design of experiments. The subsequent factors were determined to serve as regulators: curing temperature, curing time, TPOZ concentration, cerium content and TEOS molar ratio (MR) as determined by GPTMS [6]. The processing parameters that were chosen, together with their respective levels, are detailed in Table 1. The proposed L16 orthogonal array as presented in Table 2 was implemented using Minitab R16 and the Taguchi method. The rate of corrosion exhibited by the coated samples served as the foundation for the data analysis. The substrate utilized in this attempt was AA 7075-T6. The sample dimensions were 30×30×6 (mm). Using silicon carbide (SiC) paper, the specimens were ground to a fineness of 2500 grit [7]. To create consistent hydroxides and oxides on surfaces, the chemical method includes washing with soap and water, ultrasonic washing in a 0.3 M solution of sodium hydroxide, cleaning with acetone and distilled water and then activating in a solution of nitric acid at a concentration of 5 % by volume [8]. After being rinsed with distilled water and subjected to activation and cleaning with an alkaline solution, the specimens were left to dry naturally in the air [9].

Table 1: Input parameters and its levels

Parameters	Label	Level			
		1	2	3	4
Cure temperature (°C)	T	100	120	140	160
Cure duration (min)	D	210	150	120	90
TEOS/GPTMS molar proportion	R	1/1	1/2	1/3	1/4
Cerium content (g/l)	C	0	6	12	24
TPOZ content (% mol)	Z	0	12	18	24

Table 2: Design of experiments with L16 orthogonal array

Sample ID	T	D	R	C	Z
S1	1	1	1	1	1
S2	1	2	2	2	2
S3	1	3	3	3	3
S4	1	4	4	4	4
S5	2	1	2	3	4
S6	2	2	1	4	3
S7	2	3	4	1	2
S8	2	4	3	2	1
S9	3	1	3	4	2
S10	3	2	4	3	1
S11	3	3	1	2	4
S12	3	4	2	1	3
S13	4	1	4	2	3
S14	4	2	3	1	4
S15	4	3	2	4	1
S16	4	4	1	3	2

Coatings were synthesized by employing the sol-gel technique on Silicon/Zirconium organic-inorganic hybridized materials fixed with cerium inhibitor. Solutions of silicon and zircon were created independently. Combining GPTMS and TEOS with glacial acetic acid (CH3COOH) at a molar proportion of 1/3 was performed. A 1/4 MR of distilled water to GPTMS and TEOS was used while adding the water dropwise to the mixture [10]. Zr (IV) n-propoxide and CH3COOH were used to make the Zr sol. The ratio of TPOZ to CH3COOH was determined to be 1/4. The Zr sol was created by adding distilled water at a 1/5 MR to TPOZ. For half an hour, the mixture was whisked. Afterwards, the Zirconium sol was gradually mixed with the Silicon sol while stirring. After that, the blend was covered and whisked for a further hour. The last step was to add cerium nitrate and mix for 30 minutes [11]. Sixteen solutions were generated using varying concentrations of TEOS /GPTMS, TPOZ and cerium nitrate, as shown in Table 2. The solutions were allowed to mature for 2 days in a sealed container. After submerging AA7075 substrates in the solvent for 100 seconds, they were removed from the solvent. A constant speed of 18 cm/min was used for the withdrawal. Following the removal, the specimen was air-dried for 60 minutes and subsequently oven-dried for 75 minutes at 60 °C [12] and cured.

An attenuated total reflection-Fourier transform infrared spectra were used to evaluate the hybrid coatings (Bruker TENSOR 27). The range of wave numbers from 2000 to 500 cm^{-1} was used for the measurements. The absorption mode was used for the spectra measurement. Cyclic polarization testing was conducted utilizing an EG&G model 273A potentiated galvanostatic, integrated with M352 software [13]. The research utilized a 3-electrode cell with a 1 cm^2 surface area. The experimental apparatus consisted of the following elements: a platinum counter electrode, a saturated calomel reference electrode (SCE) and working electrodes consisting of the bare alloy and coated samples [14]. As the test solution, 3.5% wt. Sodium chloride (NaCl) was utilized. A scan rate of 2mV/s was utilized to experiment with room temperature. Before commencing any measurements, the coated specimen was submerged in the NaCl for an adequate period of time to achieve a steady state [15]. Each sample underwent 2 polarization measurements. The corrosion rate (CR) was determined [16] using,

$$\mathrm{CR}(mm/\mathrm{y}) = 0.00328\left(\frac{\mathrm{EW}}{d}\right)\left(\frac{I_{\mathrm{corr}}}{\mathrm{A}}\right) \quad (1)$$

Where, A = exposed surface area (cm^2), I_{corr} = corrosion current (μA), EW = equivalent weightage and d = density g/cc. Inductively coupled plasma (ICP) optical emission spectroscopy was employed subsequent to the corrosion tests in order to quantify the amounts of magnesium and aluminium ions in the NaCl solution test. The EW, was calculated using ASTM G102 [17],

$$EW = 1/\sum \frac{nf_i}{w_i} \quad (2)$$

Where, f_I = mass fraction, w_i = atomic weightage, n_i = valence and i= element in the AA7075.

3. Results and discussions

The cyclic potentio-dynamic (CPD) polarization is analysed in the study. Figs. 1 (a-i) depict the CPD curvatures for uncoated AA7075 and 16 coated samples respectively. Eqn. (2) was utilized to determine EW following a polarization test using ICP data. In the EW calculation, components comprising no more than 1% of the alloy are often incorporated. The ICP technique was

utilized to determine the mass % of Aluminium and Magnesium liberated in a 3.5% NaCl solution, subsequent to the polarization test [18]. The computed outcomes are displayed in Table 3. Table 4 gives a list of electrochemical properties determined from polarization curvatures and their signal-to-noise (S/N) ratio. The Taguchi method was employed to optimize the coating parameters through the S/N ratio. To achieve the "smaller is better" objective, the S/N ratio was computed using [19-20],

$$S/N = -10\log\left[\frac{1}{n}\left(\sum_1^n y_i^2\right)\right] \quad (3)$$

Where, y_i = value of experimental outcome in CR and n = no of measuring in each trial. In general, it was observed that coated samples exhibited I_{corr} and CR values that were reduced in comparison to AA7075. The CR of the coated AA7075 sample was seen to be four orders of magnitude lower than that of the naked AA 7075 sample. Due to the obstruction of the penetration channel, corrosion initiator penetration through the layer and to the substrate surface was diminished. By including zirconium and cerium in the composition of the coating, it is possible to improve the barrier properties and strengthen the inorganic network [21-23]. By this means, the coatings' anti-corrosion characteristics are enhanced. The CR was reduced in coatings that incorporated a greater amount of Ce nitrate. As seen in Figs. 1 (b-i), the corrosion current density increased with the presence of surface fractures in samples; furthermore, the existence of cracks rendered the samples conductive.

Table 3: EW of AA7075 and with various coatings of samples

Sample ID	EW (g/eq)	Sample ID	EW (g/eq)
AA7075	13.067±0.012	S9	12.488±0.016
S1	12.336±0.009	S10	12.476±0.021
S2	12.192±0.022	S11	13.061±0.014
S3	12.427±0.013	S12	13.018±0.017
S4	11.004±0.021	S13	13.006±0.010
S5	12.252±0.012	S14	12.382±0.013
S6	10.935±0.010	S15	12.634±0.009
S7	10.282±0.011	S16	13.010±0.012
S8	12.262±0.018		

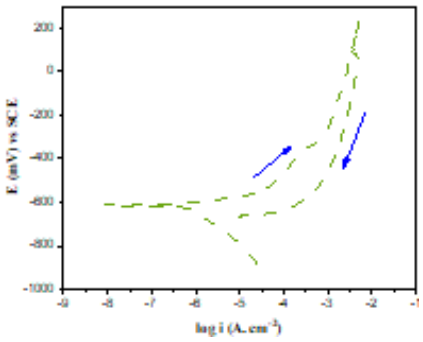

Fig. 1(a): CPD of AA7075

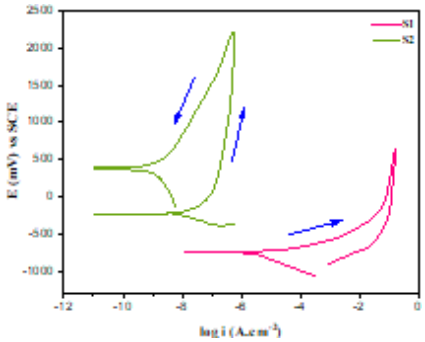

Fig. 1(b): CPD of S1 & S2

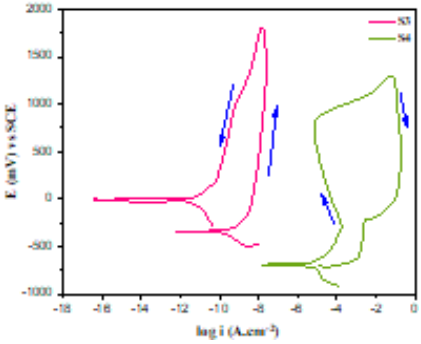

Fig. 1(c): CPD of S3 & S4

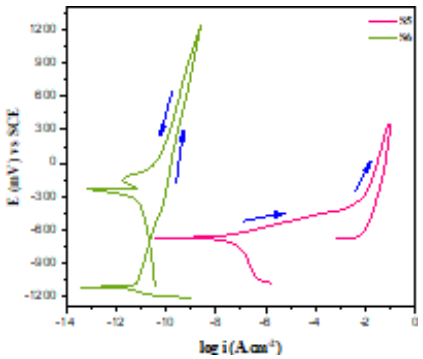

Fig. 1(d): CPD of S5 & S6

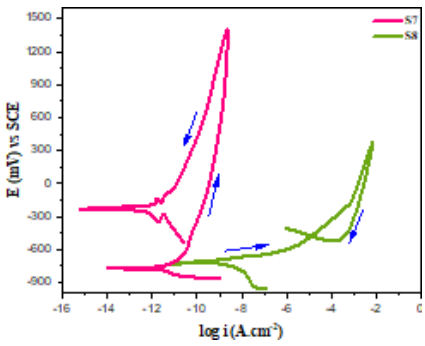

Fig. 1(e): CPD of S7 & S8

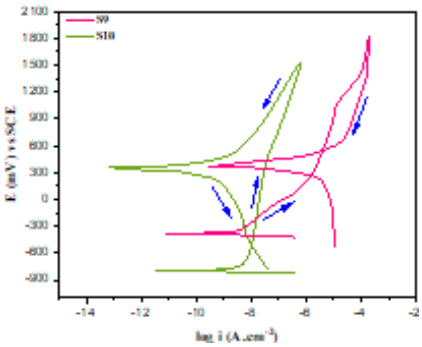

Fig. 1(f): CPD of S9 & S10

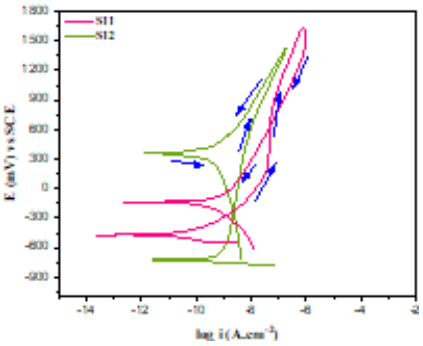

Fig. 1(g): CPD of S11 & S12

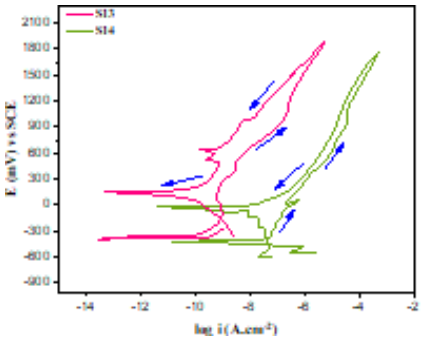

Fig. 1(h): CPD of S13 & S14

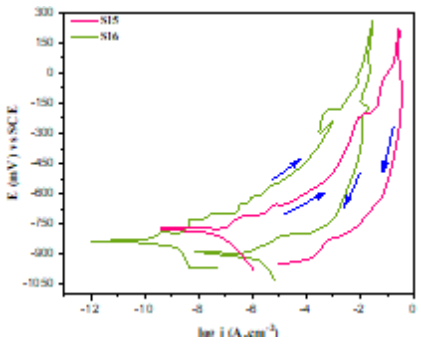

Fig. 1(i): CPD of S15 & S16

The coated samples exhibited a corrosion current density comparable to that of uncoated AA7075. On the contrary, passive area was detected in the CPD curves of other samples, indicating that these coatings possess favourable barrier qualities. Samples devoid of cracks and containing cerium exhibited a negative hysteresis loop, rendering them impervious to localized corrosion [24, 25]. This may be the result of cerium's inhibitory influence on corrosion. The formation of pits in these samples induces the formation of insoluble chemicals near the pits, which impede the pits' progression. Reverse anodic scanning revealed a reduced corrosion current density in these samples compared to forward scanning. The findings indicated that the cerium content in cracked coatings was inadequate to repair complete defects (including pits and cracks in the covering) and inhibit pitting corrosion.

Table 4: Electrochemical properties of uncoated AA 7075 and alloys with various coatings

Sample ID	I_{corr} (A/cm)	CR (mm/y)	S/N ratio
AA7075	3.343×10^{-6}	4.112×10^{-2}	33.7388
S1	3.476×10^{-6}	4.132×10^{-2}	33.696
S2	5.618×10^{-8}	7.001×10^{-4}	69.117
S3	3.48×10^{-6}	4.055×10^{-2}	33.860
S4	5.908×10^{-9}	6.791×10^{-5}	89.381
S5	3.308×10^{-6}	3.885×10^{-2}	34.232
S6	5.116×10^{-10}	4.2×10^{-6}	113.555
S7	11.276×10^{-11}	2.785×10^{-6}	117.124
S8	8.795×10^{-8}	11.363×10^{-4}	84.904
S9	3.527×10^{-9}	3.235×10^{-5}	95.822
S10	3.357×10^{-8}	3.997×10^{-4}	73.985
S11	9.174×10^{-10}	2.8×10^{-5}	97.077
S12	2.81×10^{-9}	3.31×10^{-5}	95.623
S13	10.454×10^{-9}	2.981×10^{-4}	76.533
S14	6.912×10^{-7}	8.874×10^{-3}	47.058
S15	3.506×10^{-6}	4.238×10^{-2}	33.477
S16	8.703×10^{-9}	2.727×10^{-4}	77.307

The Attenuated total reflectance - Fourier transform infrared (ATR-FTIR) spectroscopy is discussed in this study where AA7075 coatings treated with various MRs of GPTMS to TEOS are illustrated in Fig. 2 through their ATR-FTIR absorbance spectra. According to reference [26, 27] the Si-O-C band is linked to the peaks observed at 700-825 cm^{-1}. Unhydrolyzed alkoxide groups are another possible explanation for the bond. At pH~2, silanes are formed and condensation happens right after they are formed, according to researchers [28-30]. Subsequently, epoxide opening and hydrolysis form the appropriate diols. The investigation yielded a surplus of water beyond the minimum quantity required to complete the hydrolysis of alkoxide, owing to the precursor to water ratio. Therefore, it is anticipated that coating compositions will not contain any unhydrolyzed alkoxide groups. A hybridized network was formed as a result of the interaction between the Si-OH and C-OH groups of the organic networks during the hydrolysis of TEOS and GPTMS. Hydrolysis of an epoxide opens it, releasing C-OH groups. After 24 hours, around 40% of epoxide groups undergo ring opening and hydrolysis at pH 2. The observed rise in peak intensity with escalating GPTMS concentration may be attributed to the greater abundance of organic groups. Sample S1, which has a MR of TEOS to GPTMS as 1, has a diminished intensity of these bands in comparison to coatings with higher concentrations of TPOZ and GPTMS. At 1153 and 1699 /cm, 2 peaks were seen, which might have represented Zr-O-C and COO-Zr bonds, respectively. The strength of the peaks exhibited an upward trend as the TPOZ content increased. A peak at around 1810 /cm in the hybrid coatings is indicative of the Si−O−C−M or Si−O−M bond. This peak's strength was amplified when the Zr concentration rose. Overall, the peaks seen within the wavenumber range of 750-1313 /cm indicate a well-coordinated Si-O-Zr network and a favourable combination of the predecessors [31, 32].

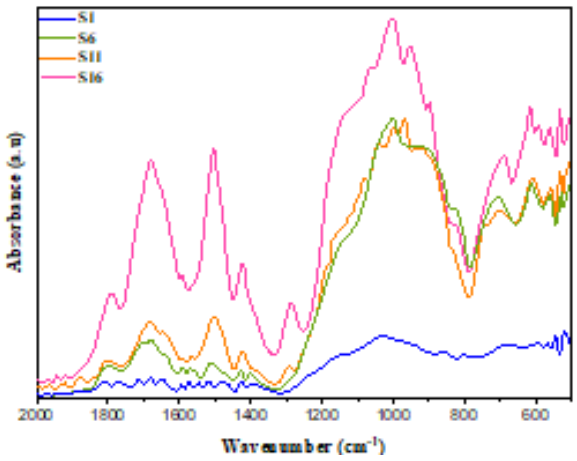

Fig. 2: Analysis of ATR-FTIR spectrum of a various samples

By utilising the S/N ratio and ANOVA analysis, the Taguchi method was able to optimise the coating conditions. The statistical analysis of the findings was conducted using the Minitab software application. In evaluating the S/N ratio, the criterion "smaller is better" was applied to reduce the CR of coatings. Fig. 3 illustrates the mean S/N ratio for each parameter across levels 1-4. The CR decreases with increasing MRs of GPTMS to TEOS, reaching a maximum of 3, as illustrated in Fig. 3. An increase in the MR of GPTMS to TEOS results in a larger quantity of organic components. By acting as network modifiers, the organic groups boost the coating structure's condensation. As a result, the coating's barrier qualities are enhanced and the AA's CR is diminished. An increase in the concentration of GPTMS led to a greater number of epoxide ring opening reactions and diol formations. The potential consequence of the elevated hydroxyl concentration is a reduction in the hydrophobicity of the film, which would render it more vulnerable to corrosion.

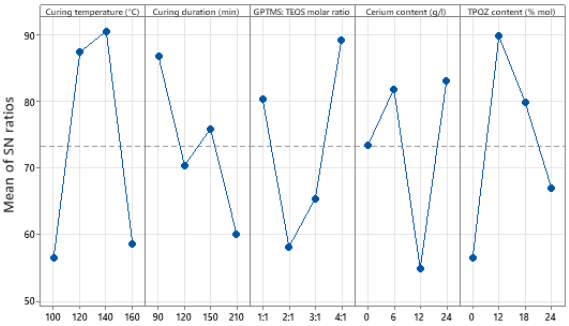

Fig. 3: Mean S/N ratio for various parameter

The trend of the influence of TPOZ concentration on CR is increasing, as illustrated in Fig. 3. The maximum CR reduction impact of TPOZ concentration is attributed to 24% mol. Up to 12 g/l of cerium nitrate added to a coating formulation accelerated the CR. This may be the result of cerium's solubility in aqueous solutions. Cerium, which is recognised for its ability to suppress corrosion, might be precipitated at the cathodic site of an AA in an appropriate concentration, therefore reducing the CR. It is possible that the concentration of cerium is inadequate to cause precipitation on the surface, hence impeding the penetration of corrosive media. The AA substrate exhibited a reduction in CR upon the introduction of 24 g/l cerium nitrate. Solvent evaporation, cross-linking and polymerization all increase in tandem with the coating's condensation as the curing temperature rises. The rate of corrosion is thereby reduced. The CR reaches its minimal value when the curing temperature reaches 120ºC. The densification kinetics of hybrid films exhibits a robust correlation with the curing time. By increasing the coatings' densification, extending the curing time to 90 minutes reduced the CR. Overall, the curing time and temperature are crucial parameters that have a substantial impact on the performance of sol-gel coatings. The CR was found to be lowest when cured for 90 minutes at 120 °C, indicating that these conditions provide the most effective protection. Alternatively stated, as the curing period was extended, a rise in the CR was seen rather than an enhancement in the performance of the coating. The best factors, as indicated by the average S/N ratio Fig. 3, are as follows: Z4, C3, T2, and D2. These factors were identified using maximum-valued average effect plots. The outcomes of ANOVA is discussed in Table 5.

Table 5: Outcomes of ANOVA

Source	df	Seq.SS 10^{-4}	Contrib.	Adj.SS 10^{-4}	Adj.MS 10^{-5}
Cure temperature (°C)	3	2.17	17.9%	2.17	7.2
Cure duration (min)	3	3.69	30.44%	3.69	12.3
GPTMS:TEOS MR	3	2.09	17.26%	2.09	7
Cerium content (g/l)	3	1.99	16.4%	1.99	6.6
TPOZ content (% mol)	3	2.18	18%	2.18	7.3
Error	0				
Total	15	12.1	100%		

Based on the mean S/N ratio, the optimal curing temperature can be determined to be 120°C. It was noticed that corrosion protection was diminished as the curing temperatures of the coatings increased and decreased. During the curing step, condensation interactions among (Silicon-hydroxyl) and (Zirconium-hydroxyl) groups might produce a network with increased cross-linking [33-35]. The possibility for improved barrier characteristics through the curing process of coatings ensures that metallic substrates are effectively protected against corrosion. Due of the higher thermal energy, an increased curing time and temperature may induce a greater number of condensation processes, resulting in a greater degree of cross-linking. Conversely, excessive baking can lead to the development of a fragile coating characterized by structural fissures. Additionally, a widespread deterioration of the hybrid film is documented [36, 37]. The elevated temperature and cure time may result in a more compact reticulated network. Potential consequences include an escalation in the quantity of fissures and degradation of the film's structure, which could ultimately lead to a reduction in its barrier properties.

To examine the quality attributes, confirmation experiments employing the optimal factor levels constitute the final phase of the Taguchi technique. Calculating the projected S/N ratio under optimal process conditions is possible using [38, 39],

$$S/N_{\text{predicted}} = S/N_{\text{m}} + \sum_1^n \left[S/N_{\text{j}} - S/N_{\text{m}}\right] \quad (4)$$

$$S/N_{\text{predicted}} = S/N_{\text{m}} + \left[S/N_{A3} - S/N_{\text{m}}\right] + \left[S/N_{B4} - S/N_{\text{m}}\right] + \left[S/N_{C4} - S/N_{\text{m}}\right] + \left[S/N_{D2} - S/N_{\text{m}}\right] + \left[S/N_{E2} - S/N_{\text{m}}\right] \quad (5)$$

Where, S/N_m = mean of all S/N ratios, S/N_j = the optimal S/N ratio for each parameter, n = no of processing factors that significantly influence the overall S/N. The projected (S/N) was achieved at 133.671. The objective function utilised to determine the CR was of the "smaller-the-better" variety. Hence, the CR under ideal conditions was computed by employing the anticipated S/N ratio using [40,41],

$$S/N_{\text{precticted}} = -10\log\left[\frac{1}{n}\left(\sum_1^n y_{\text{exp}}^2\right)\right] \quad (6)$$

Where, n = number of measurements and y_{exp} = is the predictable value of the quality feature, which in this case is the CR. Based on the computed value, the CR anticipated for the sample that was coated under ideal circumstances was 2.072×10^{-7} (mm/y). Experiments were not designed to involve optimal coating conditions. As a result, the coating was formulated and examined under the anticipated optimal circumstances. Following the fabrication of the coating under the expected optimal circumstances, ATR-FTIR and polarization tests were performed on the samples.

Fig. 4 illustrates the absorbance spectra obtained using ATR-FTIR for the optimal coating. The existence of bands spanning from 715 to 1215 /cm provides confirmation that a mixed organic-silicone oxide-zirconium (Si-O-Si, Si-O-Zr) network has formed. Absorption peaking at around 3060 cm^{-1} indicates the existence of the CH2 group integrated into the silica group. The existence of this hydrocarbon unit indicates that the coated macromolecular chains have undergone a degree of planarization [42, 43].

The 10 µm was the optimal thickness for the coating. Producing coatings with a thickness above 1 µm by the sol-gel process is a significant challenge due to the occurrence of cracking. However, an optimized process parameter combination and organic-inorganic composition allowed for the development of a hybrid coating with a larger thickness. A greater thickness of coating resulted in an augmentation of the protective effect of the coating. A more substantial layer of coating inhibits the ingress of corrosive substances and offers an enhanced barrier function. Table 6 and Fig. 5 depict the outcomes of the spectrum of AA7075 substrate with optimal coating and cyclic polarization test. According

to the study's findings, the ideal coating would have pitted corrosion resistance and a negative hysteresis loop. The coated AA 7075 exhibited a CR that was five orders of magnitude lower than that of the untreated alloy, even under ideal conditions. The experimental findings of the corrosion test and the Taguchi method's prediction for the optimal coating were in excellent agreement [44, 45].

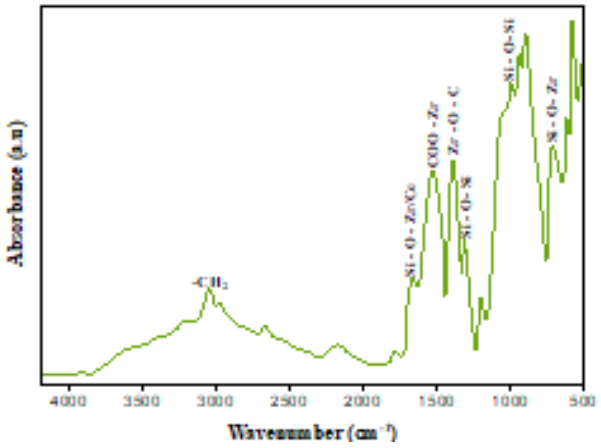

Fig. 4: ATR-FTIR spectra of AA7075 with optimal coating

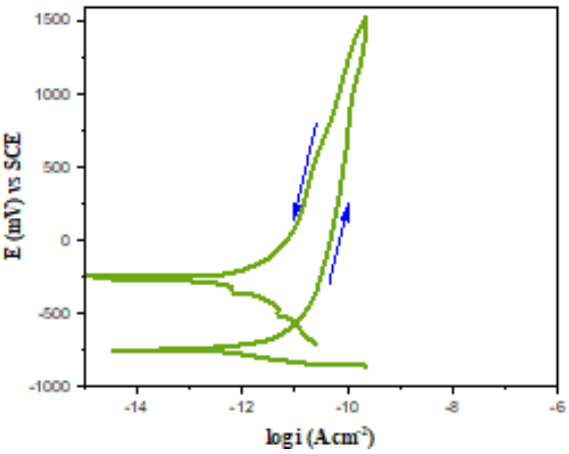

Fig. 5: CPD of AA7075 for optimal coating in a 3.5% NaCl solution

Table 6. Polarization test results for AA 7075 with optimal coating

Result	Value
Icorr (A/cm^2)	$1.597\times10^{-11}\pm0.030$
CR (mm/y)	$2.092\times10^{-7}\pm0.025$
E_{corr} (mV vs SCE)	-685±12
EW (g/eq)	11.906±0.009

4. Conclusion

Different circumstances were utilized to produce hybridized organic-inorganic coatings using sol-gel dip-coating. Process parameter optimization was accomplished utilizing the Taguchi design approach with an L16 orthogonal array. ANOVA was used to assess the experimental outcomes. In accordance with the findings, the CR of coated AA7075 was most significantly influenced by the molar proportion between GPTMS and TEOS. The incorporation of a greater number of organic components into the coating structure was facilitated by a higher MR of GPTMS to TEOS. The presence of organic groups on the substrate of AA enhances condensation inside the coating structure and decreases the rate of corrosion. The CR exhibited a reduction as the TPOZ level increased. Elevated durations and temperatures during overbaking can result in a reduction of the coating's barrier properties, hence hastening the corrosion of the substrate alloy. However, it is observed that the rate of corrosion diminishes with increasing curing time and temperature, which are 120 °C and 90 minutes, respectively. By optimizing the parameters listed below: The CR was significantly reduced to an absolute minimum when a R of 1/3, Z of 24% mol, C of 24 g/l, T of 120 °C and D of 90 minutes were utilized. The confirmation test outcomes under ideal conditions shown a high degree of concurrence with the predictions generated by the Taguchi method. By optimizing process conditions and coating composition, the CR of AA7075 was significantly diminished from an approximate value of 0.03 mm/y to 0.03×10^{-5} mm/y. Similar outcomes can be observed with analogous hybrid sol-gel coatings. The optimal coating that was formulated offers effective barrier qualities for AA7075, rendering it impervious to pitting corrosion.

REFERENCES:

[1] J. Mokhtarian, A. Allafchian and M. Atapour. 2018. Effect of silane coating containing SiC nanoparticles on the corrosion behaviour of stainless steel 304, *Micro & Nano Letters*, 13(8), 1057-1226. https://doi.org/10.1049/mnl.2018.0049.

[2] M. Bahrami, G.H. Borhani, S.R. Bakhshi and A. Ghasemi. 2017. Optimization of effective processing parameters of hybrid anti-corrosion Si/Zr sol-gel coatings doped with cerium salt for aluminum alloy 6061, *J. Solgel Sci. & Tech.*, 81(3), 921-933. https://doi.org/10.1007/s10971-016-4255-1.

[3] K. Mathivanan, D. Thirumalaikumarasamy, M. Ashokkumar, S. Deepak and M. Mathanbabu. 2021. Optimization and prediction of AZ91D stellite-6 coated magnesium alloy using Box Behnken design and hybrid deep belief network, *J. Mater. Res. & Tech.,* 15(1), 2953-2969. https://doi.org/10.1016/j.jmrt.2021.09.069.

[4] A. Duran, Y. Castro, A. Conde and J.J.D. Damborenea. 2018. *Sol-Gel Protective Coatings for Metals*, Handbook Sol-Gel Sci. & Tech.: Processing, Characterization & Applications, Springer Nature, 2369-2433. https://doi.org/10.1007/978-3-319-32101-1_70.

[5] K.P. Kumar, R. Vasanthakumar, V. Vimala, P. Naveenkumar, R. Mohan, S.H. Ahammad and R. Girimurugan. 2025. Multiobjective optimization on the process parameters for friction stir welded AA2024 composites using RSM and GRA, *AIP Conf. Proc.*, 3306(1), 070012. https://doi.org/10.1063/5.0276016.

[6] S. Adhami, M. Atapour and A.R. Allafchian. 2015. Corrosion protection of copper by silane sol-gel coatings, *J. Solgel Sci. & Tech.*, 74(3), 800-809. https://doi.org/10.1007/s10971-015-3665-9.

[7] H. Cheraghi, M. Shahmiri and Z. Sadeghian. 2012. Corrosion behavior of TiO_2-NiO nanocomposite thin films on AISI 316L stainless steel prepared by sol-gel method, *Thin Solid Films*, 522(1), 289-296. https://doi.org/10.1016/j.tsf.2012.07.125.

[8] L.G.S. Kumar, D. Thirumalaikumarasamy, K. Karthikeyan, M. Mathanbabu and T. Sonar. 2023. Optimization of process parameters for minimizing porosity level and maximizing hardness of AA2024 alloy coating on AZ31B alloy using computational response

surface methodology, *Int. J. Inter. Design & Mfg.,* 19(1), 67-81. https://doi.org/10.1007/s12008-023-01501-7.

[9] J.H. Liu, Z.W. Zhan, M. Yu, S.M. Li, Q. Wang, J. Zhang and M. Wang. 2012. Adsorption of glycidoxypropyl-trimethoxy-silane on α and β phases of titanium alloy Ti-6.5Al-1Mo-1V-2Zr, *Surface & Interface Analysis*, 44(7), 863-869. https://doi.org/10.1002/sia.4923.

[10] J. Qiu, E. Sakai, L. Lei, Y. Takarada and S. Murakami. 2012. Improving the shear strength by silane treatments of aluminum for direct joining of phenolic resin, *J. Mat. Processing Tech.*, 212(11), 2406-2412. https://doi.org/10.1016/j.jmatprotec.2012.07.008.

[11] M. Mathanbabu, D. Thirumalaikumarasamy and M. Tamilselvi. 2022. Optimization of plasma spray process variables to attain the minimum porosity and maximum hardness of the LZ/YSZ thermal barrier coatings utilizing the response surface approach, *Mater. Res. Express,* 9(9), 1-18. https://doi.org/10.1088/2053-1591/ac8857.

[12] S. Durai, P. Kanakarajan, N. Viswanathan, R. Vivek, S. Sakthi, R.T.J. Nirmalraj and R. Girimurugan. 2025. Investigation on the impact of tensile properties in dissimilar welds of AA5128 and AA6063 composites by FSW, *AIP Conf. Proc.,* 3306(1), 070010. https://doi.org/10.1063/5.0276195.

[13] M. Yu, L. Yuxing, L. Jianhua, L. Songmei, X. Bing, Z. You and Y. Xiolin. 2015. Effects of cerium salts on corrosion behaviors of Si-Zr hybrid sol-gel coatings, *Chinese J. Aeronautics*, 28(2), 600-608. https://doi.org/10.1016/j.cja.2015.01.011.

[14] S. Brzezinski, D. Kowalczyk, B. Borak, M. Jasiorski and A. Tracz. 2012. Applying the sol-gel method to the deposition of nanocoats on textiles to improve their abrasion resistance, *J. Applied Polymer Sci.*, 125(4), 3058-3067. https://doi.org/10.1002/app.36353.

[15] G. Krishnamoorthi, J. Mathan, L.G. Babu, G. Ravivarman, A. Sivalingam, K.N. Gunasekaran and R. Girimurugan. 2025. Investigation on the mechanical behavior of wheat straw fiber reinforced polypropylene composites, *AIP Conf. Proc.,* 3306(1), 070013. https://doi.org/10.1063/5.0276027.

[16] S. Seshaiah, D. Sampathkumar, M. Mariappan, A. Mohankumar, G. Balachandran, M. Kaliyamoorthy and R. Gopal. 2022. Optimization on material removal rate and surface roughness of stainless steel 304 wire cut EDM by response surface methodology, *Adv. in Mat. Sci. & Engg.*, 1-10. https://doi.org/10.1155/2022/6022550.

[17] J.H. Liu, Z.W. Zhan, M. Yu and S.M. Li. 2013. Adsorption behavior of glycidoxypropyl-trimethoxy-silane on titanium alloy Ti-6.5Al-1Mo-1V-2Zr, *Applied Surfaces Sci.*, 264, 507-515. https://doi.org/10.1016/j.apsusc.2012.10.054.

[18] S.C. Kundurti and A. Sharma. 2023. Evaluation of microstructural, mechanical and corrosion behaviours of laminated AA6061/AA7075 metal matrix composites build by friction stir additive manufacturing for structural applications, *Mat. Res.*, 26(1), 1-12. https://doi.org/10.1590/1980-5373-mr-2023-0176.

[19] P. Sellamuthu, J.P. Gibu, V.S. Kumar, S.M. Reddy, G. Sivaraman, A. Ramakrishnan and R. Girimurugan. 2025. Experimental investigations and optimization of process parameter through high speed hard turning process on C45 steel, AIP *Conf. Proc.,* 3306(1), 070005. https://doi.org/10.1063/5.0276022.

[20] M. Catauro, F. Bollino, R. Giovanardi and P. Veronesi. 2017. Modification of Ti6Al4V implant surfaces by biocompatible TiO_2/PCL hybrid layers prepared via sol-gel dip coating: Structural characterization, mechanical and corrosion behavior, *Mat. Sci. & Engg.: C*, 74(1), 501-507. https://doi.org/10.1016/j.msec.2016.12.046.

[21] A. Mohankumar, T. Duraisamy, D. Sampathkumar, S. Ranganathan, G. Balachandran, M. Kaliyamoorthy, M. Mariappan and L. Mulugeta. 2022. Optimization of cold spray process inputs to minimize porosity and maximize hardness of metal matrix composite coatings on AZ31B magnesium alloy, *J. Nanomaterials,* 2022, 1-17. https://doi.org/10.1155/2022/7900150.

[22] P. Satishkumar, C.S. Murthi, R. Chebolu, Y.S. Rao, R.Y. Capangpangan, A.C. Alguno, V.P. Yadav, M. Chitra and M. Gopal. 2022. Optimizing the mechanical and microstructure characteristics of stir casting and hot-pressed AA7075/ZnO/ZrO_2 composites, *Adv. Mat. Sci. & Engg.*, 2022, 1-18. https://doi.org/10.1155/2022/6559014.

[23] N. Saravanan, S. Balamurugan, V. Sureshkumar, R. Vivek, R. Mohan, S. Nanthakumar, A. Revathi and R. Girimurugan. 2025. Equilibrium and kinetic data for adsorption of methylene blue onto nickel ferrite nanocomposites., AIP *Conf. Pro.,* 3306(1), 070007. https://doi.org/10.1063/5.0276023.

[24] P. Satishkumar, C.S. Murthi and R. Meenakshi. 2021. Optimization of machining parameters in wire EDM of OFHC copper using Taguchi analysis, *Mat. Today: Proc.*, 37(2), 922-928. https://doi.org/10.1016/j.matpr.2020.06.120.

[25] S. Surendran, T. Sundaram and P.S. Kumar. 2022. Optimization of surface roughness and tool wear during machining of AMMC using Taguchi technique, *Chiang Mai J. Sci.*, 49(6), 1653-1662. https://doi.org/10.12982/CMJS.2022.095.

[26] B. Ramesh, S. Sathishkumar, A.H. Elsheikh, S. Mayakannan, K. Sivakumar and S. Duraithilagar. 2022. Optimization and experimental analysis of drilling process parameters in radial drilling machine for glass fiber/nano granite particle reinforced epoxy composites, *Mat. Today: Proc*, 62(2), 835-840. https://doi.org/10.1016/j.matpr.2022.04.042.

[27] V.S. Kumar, M. Amarnath, V.M. Madhavan, L. Girisha, P. Vijayakumar, A.M. Appusamy and R. Girimurugan. 2025. Investigation on the mechanical and thermal properties of coconut shell powder and HDPE composites, *AIP Conf. Proc.,* 3306(1), 070009. https://doi.org/10.1063/5.0276194.

[28] R. Srinivasan, S. Karunakaran, M. Hariprabhu, R. Arunbharathi, S. Suresh, S. Nanthakumar, S.K.H. Ahammad, S. Mayakannan and M. Jayakumar. 2023. Investigation on the mechanical properties of powder metallurgy-manufactured AA7178/$ZrSiO_4$ nano-composites, *Adv. Mat. Sci. & Engg.*, 1-11. https://doi.org/10.1155/2023/3085478.

[29] B.P. Krishnan, P. Gopi, M. Mathanbabu and S. Eswaran. 2019. Experimental Investigation of Solar Drier Integrated with HSU for Crops. *J. Adv Res. in Dynamical & Control Systems,* 11(12), 167-173. http://doi.org/10.5373/JARDCS/V11I12/20193351.

[30] R. Manikandan, P. Ponnusamy, S. Nanthakumar, A. Gowrishankar, V. Balambica, R. Girimurugan and S. Mayakannan. 2023. Optimization and experimental investigation on AA6082/WC metal matrix composites by abrasive flow machining process, Article ID: S2214785323013160, *Mat. Today: Proc.*, https://doi.org/10.1016/j.matpr.2023.03.274.

[31] I. Danaee, M. Kanaani, M.H. Maddahy and S. Nikmanesh. Corrosion behavior of Ce-oxide/hydroxide

coated AA7075-T6 prepared by dip immersion method, *Turkish J. Engg. & Environmental Sci.*, 38(3), 363-372, https://doi.org/10.3906/muh-1403-12.

[32] C.J. Fu, Z.W. Zhan, M. Yu, S.M. Li, J.H. Liu and L. Dong. 2014. Influence of Zr/Si molar ratio on structure, morphology and corrosion resistance of organosilane coatings doped with zirconium (IV) n-propoxide, *Int. J. Electrochemical Sci.*, 9(5), 2603-2619. https://doi.org/10.1016/S1452-3981(23)07951-8.

[33] W. Chen, J. Hang, X. Sun, L. Jin and H. Guo. 2018. Preparation and properties of waterborne nano-Al_2O_3/polysiloxane hybrid coatings on magnesium alloy for corrosion protection, *Gaofenzi Cailiao Kexue Yu Gongcheng/Polymeric Mat. Sci. & Engg.*, 34(1), 112-118.

[34] B. Babu, N. Senniangiri, P. Lingeswaran, S. Lokesh, G. Sivaraman, N. Vijayakumar and R. Girimurugan. 2025. Characterizing the Influence of MoS2 Hybridization on the Tribological Behaviors of AZ91D-SiC Composites, *J. Physics: Conf. Series,* 3045(1), 012001. https://doi.org/10.1088/1742-6596/3045/1/012001.

[35] L. Pezzato, K. Brunelli and M. Dabalà. 2016. Corrosion properties of plasma electrolytic oxidation coated AA7075 treated using an electrolyte containing lanthanum-salts, *Proc. 7th Symp. Aluminium Surface Sci. & Tech., Surface & Interface Analysis*, 48(8), 729-738, Madeira, Portugal. https://doi.org/10.1002/sia.5983.

[36] K. Shirvani and S. Mastali. 2012. Effect of grain refinement and immersion time on morphology, topography and corrosion resistance of CCC-Coated 7075 Al alloy, *J. Electrochemical Society*, 159(2), 74-79. https://doi.org/10.1149/2.038202jes.

[37] R. Edwin, M. Lakshmanan, M. Jaiganesh and S.R.K. Rao. 2015. Effect of scandium addition on the erosion corrosion behaviour of AA7075, *J. Corrosion Sci. & Engg.*, 18(9), 1-10.

[38] K.S. Kumar, J. Srinivas, P. Ashokkumar, R. Saravanan, V. Aravind, S.S. Bhat and R. Girimurugan. 2025. Utilization of Steelmaking By-Products and Aluminum Sludges in Alkali-Activated Materials: A Sustainable Approach for Construction Applications, *J. Physics: Conf. Series,* 3045(1), 012002. https://doi.org/10.1088/1742-6596/3045/1/012002.

[39] E. Galata, C.M. Veziri, G.V. Theodorakopoulos, G.E. Romanos and E.A. Pavlatou. 2022. Composite go/ceramic membranes prepared via chemical attachment: Characterisation and gas permeance properties, *Membranes*, 12(12), 1-33. https://doi.org/10.3390/membranes12121181.

[40] B. Xue, X. Zong, C. Wang, H. Zhang and J. Luo. 2020. Adsorption behavior of GTMS on AA2024-T3 aluminum alloy and the application on surface pretreatment, *Mat. Sci. Forum*, 984(1), 31-42. https://doi.org/10.4028/www.scientific.net/MSF.984.31.

[41] A. Moorthy, K. Kanagaraj, M. Palanisamy and G. Ramasamy. 2024. Investigation of synthetic and natural cork fiber laminate polymer composite bending characteristics, *Matéria (Rio de Janeiro),* 29, 20240489. https://doi.org/10.1590/1517-7076-RMAT-2024-0489.

[42] A.C.F. Alvarez, M.A.D. Crespo, A.M.T. Huerta, H. Cong, S.B.B. Sibaja and A.B.L. Oyama. 2017. Intensification of electrochemical performance of AA7075 aluminum alloys using rare earth functionalized water-based polymer coatings, *Polymers*, 9(5), 1-23. https://doi.org/10.3390/polym9050178.

[43] F. Songur, E. Arslan and B. Dikici. 2022. Taguchi optimization of PEO process parameters for corrosion protection of AA7075 alloy, *Surface Coatings Tech.*, 434(1), 128202. https://doi.org/10.1016/j.surfcoat.2022.128202.

[44] B. Thirumaran and S.P. Kumareshbabu. 2019. Corrosion behaviour of Stir-Squeeze cast optimised AA7075 CuCNT/CuGrP reinforced metal matrix composites, *Mat. Today: Proc.*, 27(3), 2774-2781. https://doi.org/10.1016/j.matpr.2019.12.198.

[45] A. Petica, A.C. Manea, G. Mihai, I. Nicola, V. Ceara and L. Anicai. 2022. Cerium-based conversion films developed on LiAl-layered double hydroxide coatings for corrosion protection of AA7075 aluminum alloys, *J. Electrochemical Sci. & Engg.*, 12(4), 703-719. https://doi.org/10.5599/jese.1305.